Chapter 3
Numerical Simulation Method

Tomokazu Murakami

Abstract This chapter presents a description of models used for simulations performed in this book, including the Coastal ocean Current Model with a multi-sigma coordinate system (CCM) developed by the author and a colleague for computation of seawater flow, a wave model SWAN developed at Delft University of Technology, and the Lagrangian particle tracking model.

Keywords Numerical simulation · Ocean model · Wave model · Particle tracking model

3.1 Ocean Model CCM

This section presents a description of the Coastal ocean Current Model with a multi-sigma coordinate system (CCM) used in this book, developed by the author and colleagues for seawater flow computations (Murakami et al. 2004).

Seawater flow in inland seas such as Sakiyama Bay and Amitori Bay is closely involved with the vertical structure of water temperature, salinity, and density. These quantities are governed strongly by oceanic water entering from the bay mouth, as well as layering because of insolation and river water, circulation inside of the bay by wind, and upwelling. For that reason, the numerical computation of seawater flow in an inland sea requires correct evaluation not only of changes of geographical features but also the effects of meteorological fields such as insolation and wind, as well as solving from offshore to the inland sea continuously with sufficient accuracy.

This chapter is based on work reported by Murakami et al. (2004).

T. Murakami (✉)
Storm, Flood and Landslide Research Division, National Research Institute for Earth Science and Disaster Resilience, Tsukuba, Japan
e-mail: tmurakami@bosai.go.jp

S. Shimokawa et al. (eds.), *Geophysical Approach to Marine Coastal Ecology*, Springer Oceanography, https://doi.org/10.1007/978-981-15-1129-5_3

Seawater inflow from offshore is important for inland seas such as Sakiyama Bay and Amitori Bay. Accordingly, it is necessary to configure a computational domain widely including offshore areas. However, the water depth difference is highly extended between that in an inland sea and offshore in a computational domain that is so configured. Furthermore, geographical features change suddenly and intricately at the bay mouth. The σ coordinates, which implement correct expressions of complicated submarine topography and easy handling of boundary conditions, are in heavy use for the computation of seawater flow under such conditions. Ocean models using this scheme, including POM (Mellor 2004), have been developed.

The σ coordinate system is defined as

$$\sigma = \frac{z-\zeta}{\zeta+h} = \frac{z-\zeta}{H}, \tag{3.1}$$

where ζ represents the water surface displacement, h denotes the still water depth, and H stands for the total depth.

The primitive equations are converted into the σ coordinate system from the Cartesian coordinate system with Eq. 3.1. Then, they are discretized and solved using the finite difference method. The relation between the vertical difference of physical quantity in the Cartesian coordinate system ϕ and that of physical quantity in the σ coordinate system $\tilde{\phi}$ is expressed as

$$\frac{1}{\Delta z}(\phi_{k+1} - \phi_{k-1}) = \frac{1}{H}\frac{1}{\Delta\sigma}(\tilde{\phi}_{k+1} - \tilde{\phi}_{k-1}). \tag{3.2}$$

In the difference equation in the σ coordinate system of the right-hand side of Eq. 3.2, $\Delta\sigma$ is multiplied by total depth H having a horizontal variation as shown in relation $\Delta\sigma \cdot H = \Delta z$ obtained from Eq. 3.1. The difference value is calculated using Δz distorted for every lattice depending on the water depth. For example, Δz offshore with a depth of 100 m and in an inland sea with a depth of 3 m are 10 m and 0.3 m, respectively, in the configuration of 10 layers at a vertical regular interval in the σ coordinate system. The difference equation of Eq. 3.2 is apt to yield a numerical error at an enlarged Δz or when the vertical change of physical quantities is great. Accordingly, the accuracy of vertical difference deteriorates extremely offshore with a large water depth compared with an inland sea. When a physical quantity with a large numerical error is introduced from offshore into an inland sea as the target of computation, a large numerical error will arise in computation of a physical quantity in the inland sea. This difficulty requires more careful handling, especially when coupled with a meteorological field, because the vertical change of physical quantities is enhanced because of momentum transfer by wind, heat exchange by insolation, and water balance by precipitation and evaporation. Consequently, it is an important problem that the accuracy of vertical difference is dependent on water depth when solving continuously from offshore to an inland sea.

Simplified solutions to this problem include increasing the number of vertical layers and the concept of unequally spaced layers by making the interlayer spacing near the sea surface dense. However, a considerable number of vertical layers or extremely unequal layer spacing is indispensable for the method described above to reduce the differences of Δz between an inland sea and offshore. These measures are expected to increase the computation time and instability in computation. They are not conclusive solutions.

The present author and colleagues have newly proposed the multi-sigma coordinate system in which a calculation domain is divided into numerous regions along the vertical direction, and σ coordinates are applied to each region. This multi-sigma coordinate system is defined as follows, with divided regions designated sequentially from the sea surface as I, II, III, …:

$$\sigma_{\mathrm{I}} = \frac{z-\zeta}{\zeta + h_{\mathrm{I}}} \quad \text{in region I}\,(-h_{\mathrm{I}} \le z < \zeta) \tag{3.3}$$

$$\sigma_{\mathrm{II}} = \frac{S_{\mathrm{I}} + z}{h_{\mathrm{II}}} \quad \text{in region II}\,(-h_{\mathrm{II}} \le z < -h_{\mathrm{I}}) \tag{3.4}$$

$$\sigma_{\mathrm{III}} = \frac{S_{\mathrm{II}} + z}{h_{\mathrm{III}}} \quad \text{in region III}\,(-h_{\mathrm{III}} \le z < -h_{\mathrm{II}}) \tag{3.5}$$

$$\begin{cases} h_{\mathrm{I}} = h & \text{at } h \le S_{\mathrm{I}} \\ h_{\mathrm{I}} = S_{\mathrm{I}} & \text{at } h > S_{\mathrm{I}} \end{cases}$$

$$\begin{cases} h_{\mathrm{II}} = h - S_{\mathrm{I}} & \text{at } h \le S_{\mathrm{II}} \\ h_{\mathrm{II}} = S_{\mathrm{II}} - S_{\mathrm{I}} & \text{at } h > S_{\mathrm{II}} \end{cases}$$

$$\begin{cases} h_{\mathrm{III}} = h - S_{\mathrm{II}} & \text{at } h \le S_{\mathrm{III}} \\ h_{\mathrm{III}} = S_{\mathrm{III}} - S_{\mathrm{II}} & \text{at } h > S_{\mathrm{III}} \end{cases}$$

The definition of the σ coordinates of representative regions I, II, and III is described below, but this definition also applies to region IV and deeper regions. S_{I}, S_{II}, and S_{III}, respectively, represent the distance from $z = 0$ to the interface between regions I and II, II and III, and III and IV. Such S is designated as the interface depth. Figure 3.1 shows the grid points of the so-defined multi-sigma coordinates and those of the conventional σ coordinates. Conventional σ coordinates of Fig. 3.1 represent a big difference in Δz between the inland sea and offshore, influenced by water depth change. However, in the multi-sigma coordinate system, the influence of water depth change can be eliminated from region I by narrowing region I directly under the sea surface, so that Δz in the inland sea and offshore becomes uniform. Consequently, the water depth dependence of the accuracy of vertical difference in the top layer can be canceled, which is intrinsically important in coupled calculation with a meteorological field. Moreover, dividing a domain into multiple regions can cancel the water depth dependence of the accuracy of vertical difference, even in regions except near the sea bottom. Furthermore, the

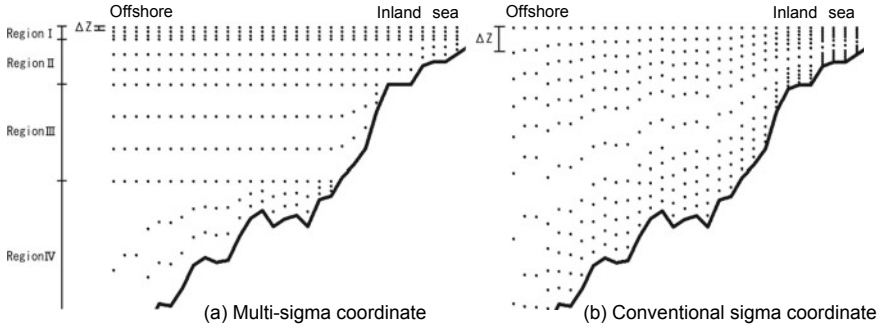

Fig. 3.1 Layouts of grid points using the multi-sigma coordinate system and the conventional sigma coordinate system. Black points signify the grid points

conventional problem of the numerical error of the horizontal pressure gradient term and horizontal diffusion term is improved because the level difference in a domain that includes no sea bottom becomes the same as that of the Cartesian coordinate system, even if geographical features are steep.

An oceanographic model using multi-sigma coordinates has been newly developed in this study. It is designated as the Coastal ocean Current Model (CCM). The major characteristics of this multi-sigma coordinate ocean model are the following.

- Hydrostatic pressure approximation and Boussinesq approximation are applied. The primitive equations include the equation of continuity, the *N*–*S* equation, the diffusion equation of temperature and salinity, and the equation of state in terms of density.
- The number of regions in which the σ coordinates is applied can be configured as arbitrary numbers.
- The fifth-order accurate upwind difference scheme is applied to the finite difference of the advective term. The fourth-order accurate central difference scheme is used for the finite difference of the diffusion term.
- The Mellor–Yamada Level 2.5 turbulent closure model (Mellor and Yamada 1982) is adopted as a turbulent model.

To investigate the usefulness of the multi-sigma coordinates, six cases of Table 3.1 were computed for Ise Bay in Japan in July 10–17, 2001 using an ocean model with the multi-sigma coordinate system.

Interface depth *S* was determined so that the number of horizontal grid points in a calculation domain was divided equally by *N* of each case. Case 1 is identical to the conventional σ coordinates.

Figure 3.2 shows the mean sea level temperature obtained using the analysis of data of a summer (July–September 2001) of the NOAA satellite. This figure shows the relative drop of the sea surface temperature only at the bay mouth. The temperature drop is regarded as taking place at the mouth where vertical mixing

Table 3.1 Cases for computation (referred from Murakami et al. 2004)

	N, Number of regions in which σ coordinates are applied	S, Interface depth (m)
Case 1	1	
Case 2	2	$S_{\mathrm{I}} = 3$
Case 3	3	$S_{\mathrm{I}} = 3$, $S_{\mathrm{II}} = 22$
Case 4	4	$S_{\mathrm{I}} = 3$, $S_{\mathrm{II}} = 19$, $S_{\mathrm{III}} = 35$
Case 5	5	$S_{\mathrm{I}} = 3$, $S_{\mathrm{II}} = 14$, $S_{\mathrm{III}} = 26$, $S_{\mathrm{IV}} = 69$
Case 6	6	$S_{\mathrm{I}} = 3$, $S_{\mathrm{II}} = 10$, $S_{\mathrm{III}} = 20$, $S_{\mathrm{IV}} = 29$, $S_{\mathrm{V}} = 55$

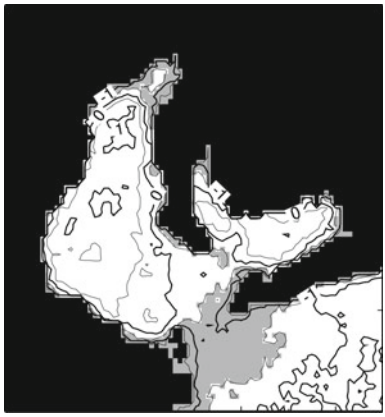

Fig. 3.2 Mean sea level temperature distribution in summer (July–September 2001); contour interval is 0.5 °C and low-temperature regions of a deviation not more than −0.5 °C are shaded (referred from Murakami et al. 2004)

prevails, although the calculation period of this study differs from the NOAA satellite analysis period. Accordingly, this phenomenon, which arises in the middle of an inland sea and offshore, is assumed as a suitable target for confirming the calculation accuracy of this model. The multi-sigma coordinate effects are examined from the viewpoint of reproducibility of this phenomenon.

Figure 3.3 shows the mean sea level temperature during the calculation period for each case. The temperature drop took place not at the mouth but offshore in Case 1. This is considered to be the result of Δz expansion offshore because of the water depth and the result of accuracy of the vertical difference deterioration. A slight temperature drop was observed at the mouth in addition to the temperature drop offshore in Case 2. This is considered to be the result of σ coordinates applied to two regions in Case 2; Δz was uniform over the inland sea and offshore near the sea surface ($z = -3$ m or above). Otherwise, in a deep region, Δz was enlarged offshore as in Case 1. In contrast to these, the temperature drop in Cases 3–6 was observed only at the mouth as shown in Fig. 3.2. Consequently, the multi-sigma coordinates are estimated as improving the calculation accuracy. Especially in Cases 4–6, in which σ coordinates were applied to four or more domains, almost no difference is indicated from the actual temperature distribution.

Fig. 3.3 Mean sea level temperature distribution during calculation period. The contour interval is 0.5 °C, with shaded low-temperature regions having deviation of not more than −0.5 °C (referred from Murakami et al. 2004)

Figure 3.4 compares the calculated density at 10:00 a.m. of each case with the measured density obtained from observational data of temperature and salinity acquired once a day (in the morning) at the bay center. Results of July 11, 12, and 16 are shown when typical characteristics were observed. The observed value was reproduced well with calculation on July 11 in Cases 1–6. In contrast, the layering was poorly reproduced on July 12 when the calculated values tended to be uniform along the perpendicular direction compared with the observed value, and on July 16 when a pycnocline appeared in the observed value because of a high river flow rate.

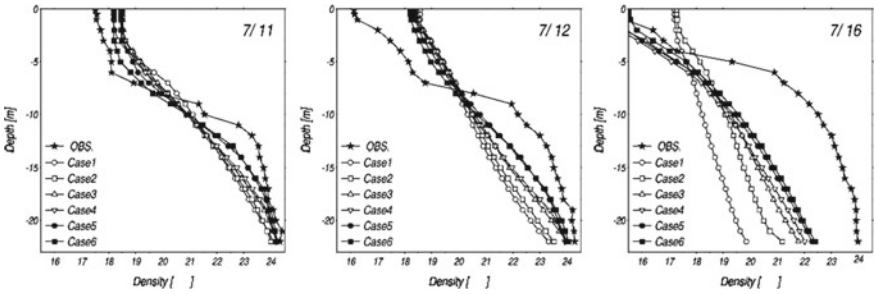

Fig. 3.4 Comparison of observed and calculated values of density distribution at point A: (left) density on July 11, (center) density on July 12, and (right) density on July 16 (referred from Murakami et al. 2004)

Calculations tended to make the density distribution too uniform along the perpendicular direction in any case. However, the density distribution of Cases 5 and 6 was approached. The calculation accuracy improved with all days as the σ coordinates were multiplexed more from Case 1 to Case 4.

Figure 3.5 shows the mean density distribution during the calculation period at cross section B of Fig. 3.1 for each case. This figure shows a difference in the density of seawater flowing in from offshore in each case (near $x = 50$ km in the figure). Thereby it is demonstrated that a difference occurred in the distribution of high-density water mass existing near the sea bottom of the inland sea. Moreover, the density contours fluctuated greatly in accordance with geographical features near the mouth in Cases 1–3. It is unnatural that the time-averaged density field fluctuates greatly depending on the water depth. It is regarded as a calculation difficulty. Actually, this difficulty is resolved gradually as the σ coordinates are multiplexed.

Figure 3.6 shows the surface residual current during the calculation period for each case. The trend of runoff to the west and inflow from the east, the characteristic of Ise Bay in the summer, is evident in the residual current field of the inland sea in all cases. However, a difference exists in the flow velocity of inflow from the east. A large vortex is observed near the open boundary of southwest and northeast in Cases 1 and 2. These vortices are known to appear on the open boundary even if a calculation domain is modified. They have been regarded as a calculation-related problem. These vortices cause an intense southwestward flow offshore. These vortices shrink in Case 3 and almost disappear in Cases 4–6. The flow offshore turns northeastward opposite to Cases 1 and 2. Consequently, it is regarded as one reason why the calculation accuracy of quantities such as temperature, salinity, and the density in the inland sea was improved that the calculative error near an open boundary was reduced using multi-sigma coordinates.

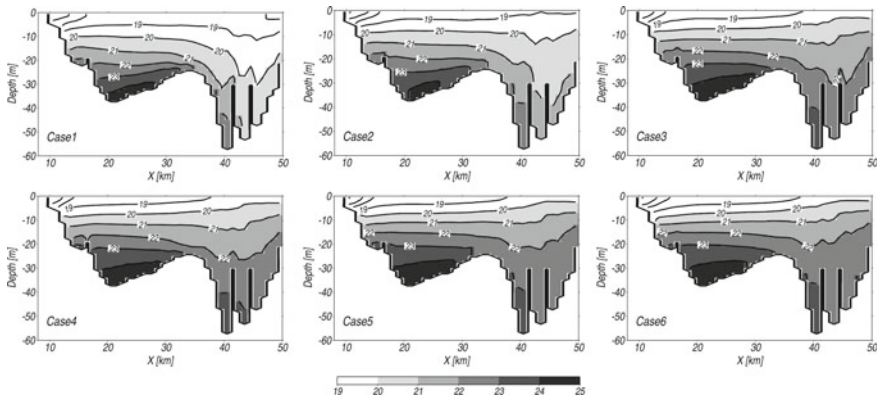

Fig. 3.5 Mean density distribution during the calculation period at cross section B. The contour interval is 1(σ_t) (referred from Murakami et al. 2004)

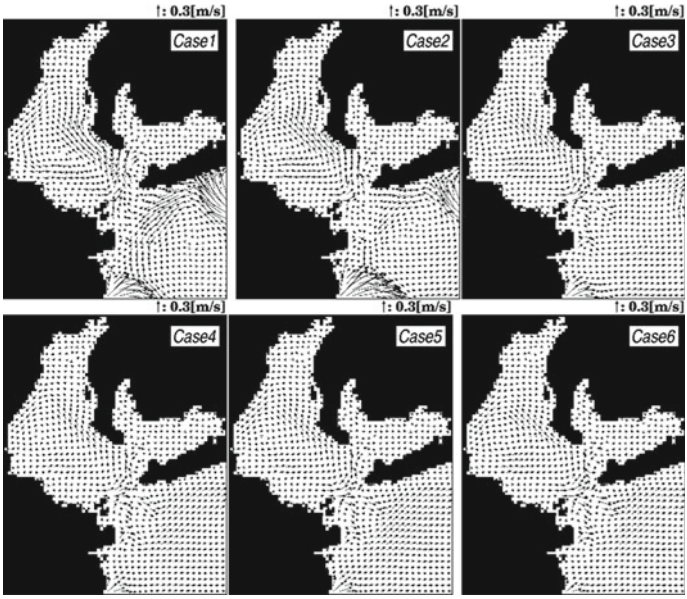

Fig. 3.6 Surface residual current during calculation period (referred from Murakami et al. 2004)

Consequently, results verified that the CCM is a suitable model for computing seawater flow, water temperature, salinity, and density in inland seas such as Sakiyama Bay and Amitori Bay, as described above.

3.2 Wave Model SWAN

SWAN (Booij et al. 1996) was used to calculate a wave field. SWAN is a wave forecasting and hindcasting model for shallow sea areas of the third-generation developed at Delft University of Technology. This section presents a description of the SWAN outline (Cycle III ver. 40.31) (Holthuijsen et al. 2004).

Because the directional wave spectrum is not conserved but the wave action density is conserved in a state with a flow, SWAN uses not the directional wave spectrum $E(s, q)$ but the wave action density spectrum $N(s, q)$, for which the independent variables are relative frequency s and wave direction q, and $N(s, q) = E(s, q)/s$. Actually, SWAN provides users with primitive equations of two types: a rectangular coordinate system and the spherical coordinate system. The primitive equation of the rectangular coordinate system is given as the following equation.

$$\frac{\partial}{\partial t}N + \frac{\partial}{\partial x}c_x N + \frac{\partial}{\partial y}c_y N + \frac{\partial}{\partial \sigma}c_\sigma N + \frac{\partial}{\partial \theta}c_\theta N = \frac{S}{\sigma} \tag{3.6}$$

In that equation, c_x, c_y, c_σ, and $c_{\theta,}$ respectively, denote the propagation velocities on the real space and the spectrum space x, y, s, and θ. They are used as components in the equations shown below using phase velocity of each component wave c, group velocity c_g, steady flow velocity vector $\overrightarrow{U} = (U, V)$, and wave number vector $\vec{k} = \left(k_{x,} k_y\right)$.

$$c_x = c_g \cos\theta + U \tag{3.7}$$

$$c_y = c_g \sin\theta + V \tag{3.8}$$

$$c_\sigma = \frac{\partial}{\partial_t}\left(\sqrt{gk\tan h(kh)} = \vec{k}\cdot\overrightarrow{U}\right) \tag{3.9}$$

$$c_\theta = \frac{c_g}{c}\left[\sin\theta\frac{\partial c}{\partial x} - \cos\theta\frac{\partial c}{\partial y}\right] - \frac{1}{k}\left(\sin\theta\frac{\partial}{\partial x} - \cos\theta\frac{\partial}{\partial y}\right)\left(\vec{k}\cdot\overrightarrow{U}\right) \tag{3.10}$$

The first term of the left-hand side of Eq. 3.6 expresses the temporal rate of change of wave action density. The second and third terms express the spatial propagation of wave action density. c_x and $c_{y,}$ respectively, represent the propagation velocity along the x-direction and y-direction. The fourth term denotes the change of relative frequency according to the temporal change of water depth and a flow (propagation velocity in s space c_σ). The fifth term expresses wave refraction by water depth and a flow (propagation velocity in θ space c_θ). S on the right-hand side (= S (s, q)) is an energy source function representing the effects of wave generation, wave dissipation, and interaction between nonlinear wave components. This function S will be described later. Equations of propagation velocity (3.7)–(3.10) are derived using the linear kinematic wave theory (Whitham 1974; Dingemans 1997; Mei 1983). Equation (3.6), the wave action density equation in the rectangular coordinate system, is converted to the spherical coordinate system on the Earth as

$$\frac{\partial}{\partial t}N + \frac{\partial}{\partial \lambda}c_\lambda N + (\cos\varphi)^{-1}\frac{\partial}{\partial \varphi}c\varphi\cos\varphi N + \frac{\partial}{\partial \sigma}c_\sigma N + \frac{\partial}{\partial \theta}c_\theta N = \frac{S}{\sigma} \tag{3.11}$$

where c_λ, c_φ, c_σ, and c_θ are given, respectively, as shown below.

$$c_\lambda = \frac{c_g \sin\theta + V}{R\cos\varphi} \tag{3.12}$$

$$c_\varphi = \frac{c_g \cos\theta + U}{R} \tag{3.13}$$

$$c_\sigma = \frac{\partial}{\partial t}\left(\sqrt{gk\tan h(kh)} - \vec{k}\cdot\vec{U}\right) \tag{3.14}$$

$$c_\theta = \frac{c_g \sin\theta\tan\varphi}{R} + \frac{1}{kR}\left(\sin\theta\frac{\partial}{\partial\varphi} - \frac{\cos\theta}{\cos\varphi}\frac{\partial}{\partial\lambda}\right)\left(\sqrt{gk\tan(kh)} - \vec{k}\cdot\vec{U}\right) \tag{3.15}$$

Therein, φ, λ, and R, respectively, denote the latitude, longitude, and the Earth's radius. Energy source function S on the right-hand side of Eqs. 3.6 and 3.11 is expressed as shown below.

$$S(\sigma,\theta) = S_{\text{in}} + S_{\text{ds}} + S_{\text{br}} + S_{\text{bf}} + S_{\text{nl}} + S_{\text{tri}} \tag{3.16}$$

In that equation, S_{in} represents an energy transport term from wind to wave, S_{ds} denotes an energy dissipation term by whitecap breaking wave, S_{br} expresses an energy dissipation term by shallow water breaking wave, S_{bf} stands for an energy dissipation term by bottom friction, S_{nl} signifies an energy transport term by nonlinear interaction between four-wave components, and S_{tri} is an energy transport term by nonlinear interaction between three-wave components. An important characteristic of SWAN is that it takes S_{br} and S_{tri} into consideration directly.

Integration of the action balance equation in SWAN is conducted using a finite difference scheme in all five dimensions (time, real space, and spectrum space). The computation time is divided using a single time step for the simultaneous integration of the propagation term and the source term. The real space is also divided using a rectangle grid with fixed resolution Δx and Δy, respectively, along the x-direction and y-direction. The spectrum space is divided by a fixed directional division $\Delta\theta$ and relative frequency $\Delta\sigma/\sigma$ (logarithmic distribution). The range of the frequency spectrum, which can be chosen freely, is divided within a range, with the low-frequency and high-frequency portions cut off.

3.3 Particle Tracking Model

The three-dimensional particle tracking model used in this book is a numerical model that tracks each particle in a Lagrangian way. Particle tracking calculations are conducted based on a seawater flow field acquired from the CCM ocean model described above. The following conditions are imposed in the case of particle tracking: (1) Diffusion is not considered, (2) particles do not jump out of the sea surface, and (3) particles perform total reflection on a boundary with land. This numerical model can track virtual particles (water particles) having no mass. It is unaffected by specific gravity. It moves only by seawater flow. Soil particles form sediment with their own weight with the effects of specific gravity considered.

Acknowledgements This research was supported by JSPS KAKENHI Grant Number 18K04377.

References

Booij N, Holthuijsen LH, Ris RC (1996) The SWAN wave model for shallow water. In: Proceedings of 25th international conference on coastal engineering, vol 1, pp 668–676

Dingemans MW (1997) Water wave propagation over uneven bottoms. Part 1—linear wave propagation. In: Advanced series on ocean engineering (vol 13). World Scientific, p 471

Holthuijsen LH, Booij N, Ris RC, Haagsma IJG, Kieftenburg ATMM, Kriezi EE, Zijlema M, van der Westhuysen AJ (2004) SWAN Cycle III Ver. 40.31 User Manual

Mei CC (1983) The applied dynamics of ocean surface waves. Wiley, New York, p 740

Mellor GL (2004) Users guide for a three-dimensional, primitive equation, numerical ocean model, 56 pp. http://www.aos.princeton.edu/WWWPUBLIC/htdocs.pom

Mellor GL, Yamada T (1982) Development of a turbulence closure model for geophysical fluid problems. Rev Geophys Space Phys 20(4):851–875

Murakami T, Yasuda Y, Ohsawa T (2004) Development of a multi-sigma coordinate model coupled with an atmospheric model for the calculation of coastal currents. Ann J Coast Eng JSCE 51:366–370 (in Japanese with English abstract)

Whitham GB (1974) Linear and nonlinear waves. Wiley, New York, p 636